Hippocampal Ripples linked to Declarative Memory Judgments in Children

Yitzhak Norman[1,2,*] Georg Dorfmüller[3], Delphine Taussig[3], Nathalie Dorison[3], Martine Fohlen[3], Mathilde Chipaux[3], Sarah Ferrand-Sorbets[3], Christine Bulteau[3], Michal Harel[1], Rafael Malach[1,4], Mikael Levy[3,4]

[1] Department of Brain Sciences, Weizmann Institute of Science, Rehovot, 76100, Israel

[2] Department of Neurological Surgery, University of California, San Francisco, California 94143, USA

[3] Department of Pediatric Neurosurgery, Rothschild Foundation Hospital, Paris, France.

[4] Senior authors

* Correspondence: YN (itzik.norman@gmail.com)

Abstract

Intracranial studies in adults have revealed significant roles for hippocampal ripples in human declarative memory. Yet, the developmental trajectory of ripples and their involvement in memory processes in children are currently unknown. We studied hippocampal ripple activity using intracranial recordings in 14 children (age: 6-14) undergoing epilepsy monitoring. After watching a pink panther cartoon twice, participants underwent an old/new recognition test, where they determined whether the events portrayed in short video clips (4s) originated from the cartoon they had just viewed or a different one. We found a significant increase in ripple rate specifically during clips recognized as familiar. The ripple rate remained unchanged when the same animated events were viewed as part of the original full-length screenings, outside the context of a recognition test. We conclude that like in adults, hippocampal ripples in children are robustly activated during declarative memory judgments, supporting the explicit identification of previously encountered events.

Introduction

The human brain undergoes significant structural and functional changes during childhood and adolescence (Brown and Jernigan, 2012; Gennatas et al., 2017; Lenroot et al., 2007; Shaw et al., 2008). These changes occur both in large-scale cortical networks (Dosenbach et al., 2011; Power et al., 2010) and in more localized prefrontal and medial temporal lobe (MTL) structures that support memory functions (Daugherty et al., 2016; Geng et al., 2019; Ghetti and Bunge, 2012; Ghetti et al., 2010; Johnson et al., 2018; Ofen et al., 2007; Riggins et al., 2018). Neuroimaging studies on hippocampal development have shown a heterogeneous pattern of age-related changes across different hippocampal regions and subfields (Canada et al., 2020; Ghetti and Bunge, 2012; Gogtay et al., 2006; Ofen, 2012; Riggins et al., 2018; Schlichting et

al., 2017). Such structural and functional changes – which generally exhibit a complex, non-linear, developmental trajectory – play a role in mediating age-related changes in declarative memory capabilities (Daugherty et al., 2017; Geng et al., 2019; Ghetti et al., 2010; Riggins et al., 2018; Schlichting et al., 2017; Tang et al., 2020).

While these studies have provided valuable insights into hippocampal development and its impact on memory performance, there remains a gap in our understanding of how specific hippocampal mechanisms, that selectively contribute to declarative memory processing, mature with age. One such key mechanism, that received significant attention in recent years, is the hippocampal ripple (Buzsáki, 2015). Ripples have been shown to play a pivotal role in systems memory consolidation and retrieval (Joo and Frank, 2018). They have been extensively linked to declarative memory retrieval in humans (Dickey et al., 2022; Henin et al., 2021; Khuvis et al., 2021; Kunz et al., 2022; Norman et al., 2019, 2021; Sakon and Kahana, 2022), and have been shown to support memory-guided decision making (Fernández-Ruiz et al., 2019; Jadhav et al., 2012; Shin et al., 2019) and offline memory consolidation (Maingret et al., 2016; Rothschild et al., 2017; van de Ven et al., 2016) in animal models.

However, despite this growing body of evidence for the critical mnemonic role played by ripples in the adult brain, it remains unknown whether ripples even exist in the hippocampus of young children and whether they are involved in similar functions as in the adult. Exploring the function of ripples across different age groups is crucial for understanding the general function of this vital hippocampal mechanism and how it evolves over time in relation to memory capabilities.

Results

The study is based on intra-cranial recordings in 14 patients (8 females) ranging in age from 6 to 14 years (mean ± SD: 9.46 ± 2.6; see Table S1 for additional demographic data). We focused on data obtained from 79 recording sites that were confirmed anatomically to be within the hippocampus (see Figure 1a-c and Methods).

Briefly, the task began with a 3-minute resting period, after which the participants watched two consecutive screenings of a 6.5-minute audiovisual pink panther cartoon. The two screenings were separated by an additional 3-minute resting period (Figure 1d). Subsequently, the participants underwent an old/new recognition test, in which they were presented with short video clips lasting 4 seconds each. These video clips were extracted either from the original cartoon (n=20) or from a different pink panther episode revolving around a similar theme (n=20; see Figure 1e and Methods for further details). The participants were asked to indicate for each video clip whether it was old or new to them via a button press.

The participants performed the task successfully, achieving an overall accuracy of 86.4 ± 4.9%. Memory performance did not correlate with age. Age did not significantly predict accuracy (Spearman's ρ=0.25, p>0.41) nor discriminability (d-prime) (ρ=0.16, p>0.59; Figure 1f), which aligns with previous reports on recognition performance in similar age groups (Ghetti and Angelini, 2008; Maril et al., 2010).

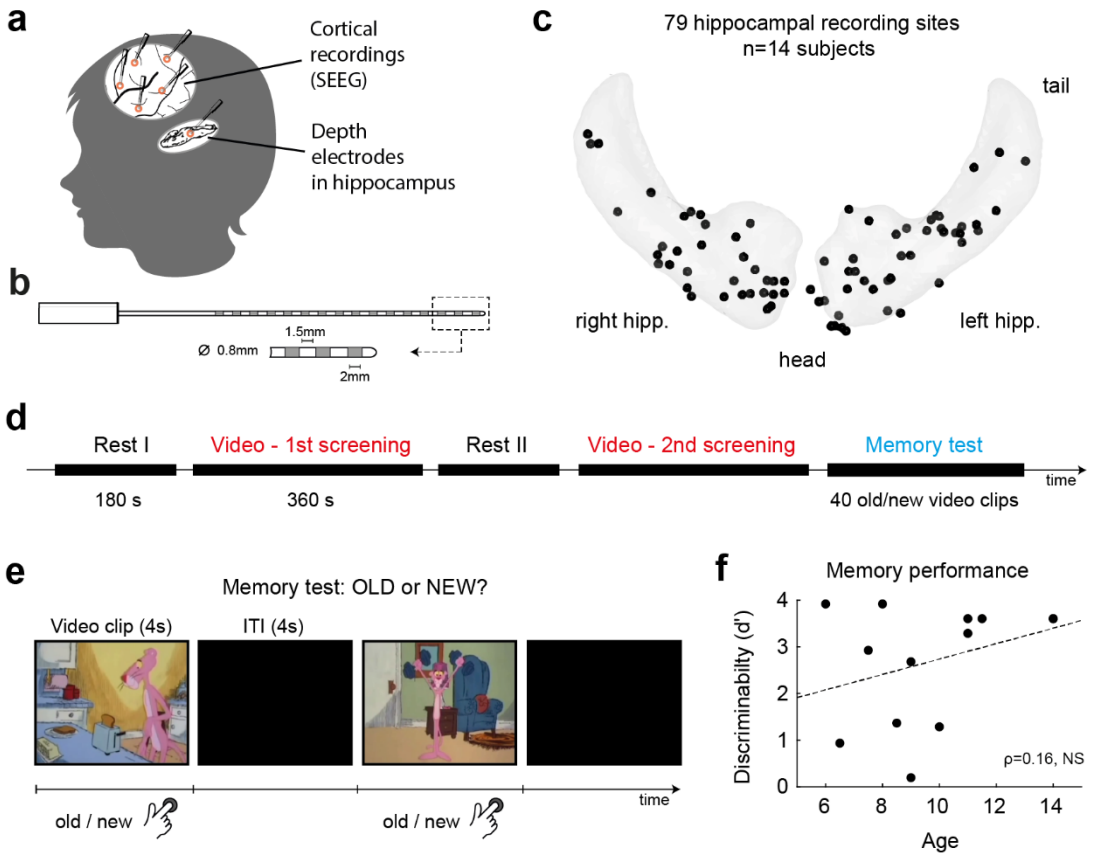

Figure 1 | Experimental design, memory performance and intracranial recordings.

(a) Each patient was implanted with multiple Stereo-EEG depth electrodes (SEEG) in the cortex and the hippocampus.

(b) Schematic diagram of a typical SEEG depth electrode.

(c) An overview of the electrodes' anatomical location. Localization was done in the native space of each patient's brain based on Freesurfer's hippocampal subfield parcellation (Iglesias et al., 2015). For the ripples analysis, only electrodes located in CA1, CA2, CA3, or the subiculum were included, resulting in a total of 79 electrodes across 14 patients.

(d) The task began with a 3-minute period of closed-eye rest, followed by a 6.5-minute viewing of a pink panther cartoon. This was followed by another rest period and a repeat viewing of the same cartoon. The recording session concluded with a recognition test.

(e) During the memory test participants were presented with 40 distinct 4-second video clips. These clips either originated from the same pink panther episode or a different one. Using a mouse button, the participants indicated for each clip whether it was familiar (old) or unfamiliar (new). Screenshots are from the Pink Panther cartoon and are used under fair use for educational purposes. Copyright: THE PINK PANTHER™ & © 1964–2023 MGM.

(f) Memory performance (d': $z(hit) - z(false\ alarm)$) among the participants was high (2.69 ± 0.36) and showed no correlation with age (Spearman's ρ=0.16, NS). Each dot represents a single participant.

Throughout the recording session, iEEG signals were acquired from the hippocampal electrodes, and ripple events were detected following standard protocols (Liu et al., 2022) that closely resemble the methods described in our earlier studies (Norman et al., 2019, 2021) (see Methods). Examples of ripple detection are depicted in Figure 2. Notably, the detected events showed a remarkably stereotypical and consistent spectral signature characterized by a brief temporal duration and a prominent increase in oscillatory power concentrated at ~90 Hz, which reflects the intense, coordinated, multi-neuron activity of hippocampal ripple events (Figure 2c-e) (Staba et al., 2004; Le Van Quyen et al., 2008).

Specifically, the hippocampal ripples recorded exhibited a peak frequency of 89.9 ± 5.5 Hz (Figure 2d) and had an average duration of 34 ± 6.4 ms. Ripple duration was determined as the time interval between the onset and the offset of the ripple, that is, when the power of the oscillatory event fell below a 2σ threshold (see Methods). The overall ripple rate throughout the experimental duration was 0.33 ± 0.01 events/sec, demonstrating a typical inter-ripple interval distribution (Figure 2f-g). For comparison with typical ripple properties in adults see (Kunz et al., 2022; Norman et al., 2019, 2021).

Applying a linear mixed-effects model to the individual electrode data, showed no significant differences in basal ripple rate, ripple duration, or ripple amplitude across the various experimental conditions (rate: $F(1,392) = 0.14$, $P = 0.71$; duration: $F(1,392) = 3.59$, $P = 0.06$; amplitude: $F(1,392) = 0.06$, $P = 0.8$), nor significant effects of age. This further emphasizes the stability of the observed stereotypical ripple properties across the participants and throughout the experiment (Chen et al., 2021). The formulation of the mixed-effects models employed was as follows:

$$x \sim condition + age + (1|subject{:}\,electrode)$$

where x is the measure of interest in each analysis (i.e., ripple rate, duration, or amplitude).

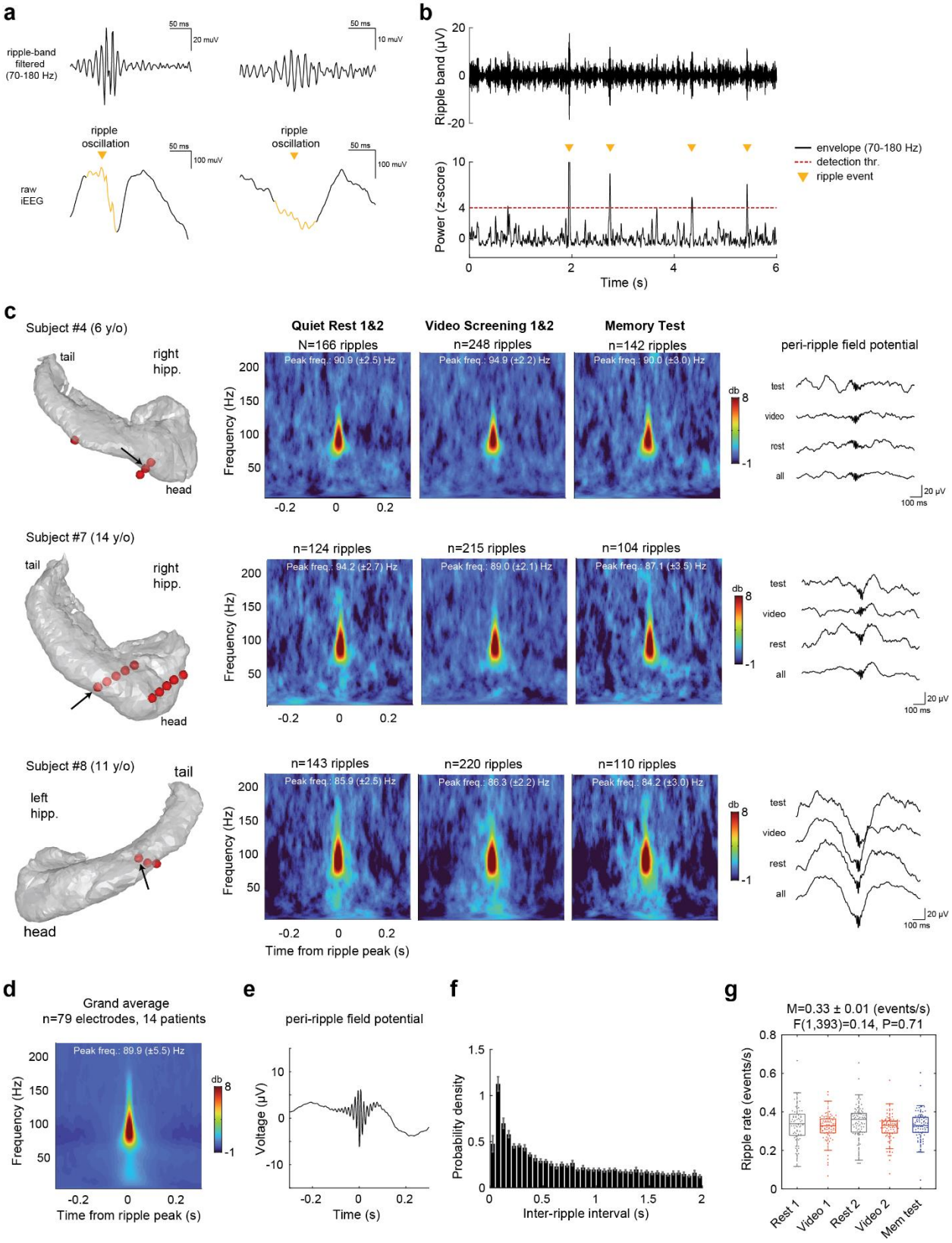

Figure 2 | Hippocampal ripples detection and their characteristics in children.

(a) Two traces of representative ripple events detected in one patient.

(b) Ripple detection procedure, showing examples of four candidate ripples (marked by orange triangle) as they appear in a CA1 recording site.

(c) Peri-ripple spectrograms and average field-potentials in representative CA1 recording sites in three patients (6, 14 and 11 years old). The left panel shows the anatomical location of each electrode within the hippocampus. Note the similar spectral signature of ripples present in these three patients, despite their varying ages. Ripples' peak frequency, duration and amplitude remain stable across the different experimental conditions: quiet rest, watching a full-length cartoon, and the memory test.

(d-e) Grand-average peri-ripple spectrogram and field-potential, computed across all hippocampal electrodes, in 14 subjects.

(f) Grand-average inter-ripple-interval distribution, in 50 ms bins.

(g) The basal (mean) ripple rate remained stable throughout the experiment, with no significant differences between task phases. However, a more transient change in ripple rate did occur during the memory test, as will be demonstrated later.

Examining ripple rate modulations during the two movie repeats and the old/new recognition test revealed four major findings, which are depicted in Figure 3. In the analysis ripple rate was computed through a peri-event time histogram (PETH) aligned to the onset of the video clips. We used 50 ms time bins smoothed by a 5-point triangular window.

Firstly, during the recognition task, there was a transient increase in ripple rate a few hundred milliseconds (half-height: 588 ± 53 ms; peak: 1015 ± 33 ms) after the onset of the video clip (clip-vs-rest: P=0.016, N=14 patients, cluster-based permutation test). This increase was evident for both clips judged as old or new (Figure 3a) and could also be observed at the single trial level, as depicted in Figure 3b.

Secondly, a significant enhancement in ripple rate was observed when the presented video clip was familiar (recognized as 'old') compared to unfamiliar (judged as 'new'). This enhancement is clearly demonstrated by comparing the blue and red curves in Figure 3a (P=0.0128, n=14 subjects, cluster-based permutation test), and by contrasting the ripple rate elicited during old and new clips individually for each subject (Figure 3c). For the latter, ripple rate was averaged over a time window of 2 s centered on the peak of the grand average response reported above (computed across all clips, old and new).

Thirdly, the observed effect exhibited a hemispheric difference, with a significantly more prominent manifestation in the left hippocampus compared to the right hippocampus. This difference is illustrated visually at the single electrode level in the old-vs-new effect size map shown in Figure 3d and statistically at the group-level in Figure 3e. In this analysis, the ripple rate was individually computed for each site, using a fixed time window of 2s centered on the peak of the grand average ripple rate response. For the

statistical comparison, we fitted a linear mixed effects model to the old-vs-new effect size values (Hedges' g), formulated as follows:

$$effectSize \sim 1 + age + hemisphere + (1|subject{:}electrode)$$

This analysis revealed a significant hemisphere effect (t(76)=3.09, P=0.003). Importantly, it also indicated the absent of an age effect (t(76) = 0.002, P = 0.96), suggesting that the recognition signal mediated by ripples is already fairly established at this school-age range. Notably, this finding aligns well with the estimated rate of neuronal maturation in the tri-synaptic circuit in humans, which is believed to reach completion before the age of 5 (Lavenex and Banta Lavenex, 2013; Seress and zljak, 1992).

Finally, by contrast with the striking increase in ripple rate responses during the recognition test, ripple rate responses observed for the same animated events when viewed in the original full-length screenings showed no enhancement (Figure 3f), neither during the first screening nor the second one. This finding suggests that the increase in ripple rate during the recognition test was specifically associated with the memory judgment being made, rather than the perception of the dynamic visual content itself.

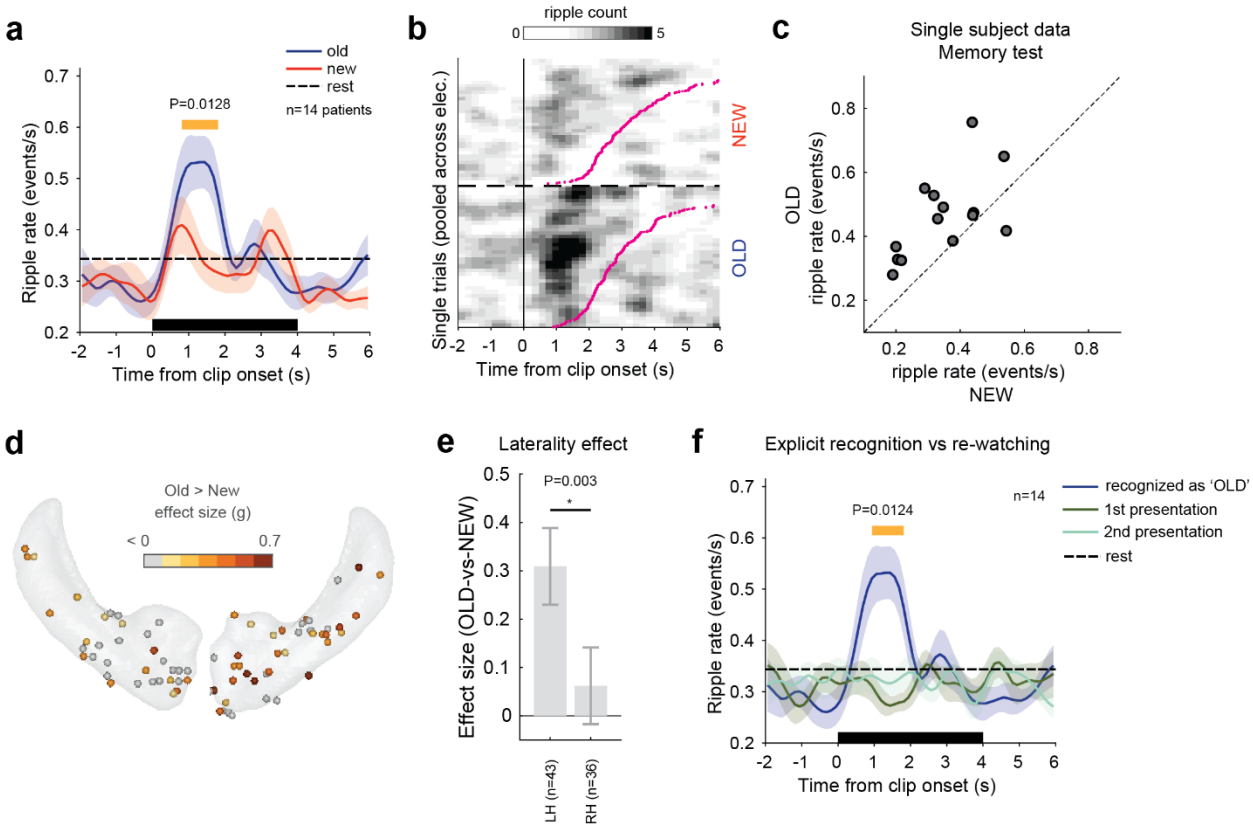

Figure 3 | Ripple rate increases during recognition of a familiar event from a cartoon.

(a) A peri-event time histogram (PETH) aligned to the clip onset was computed to show the instantaneous ripple rate modulation during the memory judgment task. The subjects were shown 4-second video clips extracted either

from the previously viewed pink panther episode ("old", n=20 clips) or from another pink panther episode ("new", n=20 clip). The results indicated that when the patients recognized a clip as familiar, there was a temporary and significant increase in the ripple rate (P=0.0128, n=14 patients, cluster-based permutation test).

(b) Hippocampal ripples density plot showing an increase in ripple probability following the presentation of a familiar ("old") clip. Trials were stacked together across all electrodes and sorted according to reaction time (pink curve). Ripples' density was smoothed using a 5-bins-wide 2d Gaussian filter for visualization purposes.

(c) Scatter plot of ripple rate in individual patients, showing "old" versus "new" clips. Except for one patient (right-hemisphere implant), all patients demonstrated a higher ripple rate when recognizing a familiar clip.

(d) Anatomical distribution of electrodes showing an old>new effect. Electrodes in the left hippocampus overall showed a stronger effect.

(e) A mixed-effects model fitted to the data showed a significant hemisphere effect, with stronger recognition-related ripple rate modulation in left compared to right hippocampus.

(f) The ripple rate demonstrated a recognition-related increase selectively during the memory test. When the same animated content was presented as part of the full-length cartoon, either during the first screening (green) or the repeated screening (turquoise), no increase in ripple rate was observed. This finding emphasizes the cognitive specificity of ripple activation, suggesting its association with the explicit memory judgment.

We next examined whether the recognition effect was specific to ripple activity or also present in other measures of local neuronal activity, particularly the high-frequency broadband power (HFB: 60-128 Hz; also known as high-gamma). The results of this analysis are presented in Figure 4. Similar to ripple rates, the HFB power displayed a transient increase during the old/new recognition test. However, in contrast to the ripple rate, this effect was less specific to the memory process, showing only a slight power increase for the old clips compared to new ones. This difference failed to reach statistical significance (P=NS, n=14 patients, cluster-based permutation test; compare Figure 4a to Figure 3a).

A direct comparison between the old-vs-new effect size of the ripple rate and the HFB power within the 4s duration of the video clips revealed a significantly stronger recognition effect for the ripple rate ($P<0.05$, n=14, Wilcoxon signed-rank test). Furthermore, even when comparing the single most recognition-selective HFB site in each patient to the single most recognition-selective ripple rate site in each patient (Figure 4e), the effect size was significantly larger for the ripple rate (P=0.0009, n=14, Wilcoxon signed-rank test). This analysis suggests that hippocampal ripples provide a more accurate reflection of the underlying mnemonic process compared to the overall population firing rate represented by HFB activity.

Finally, since HFB power and ripple rate are neuronal signals that occur within semi-overlapping frequency bands, it was important to quantify not only the disparity between the two signals, but also their association. To that end we computed the correlation between the old-vs-new effect sizes in HFB and ripple rate across all participating electrodes. This correlation was statistically significant (R=0.38, $P<0.0005$, n=79 electrodes; Figure 4f). Nonetheless, the somewhat moderate strength of this correlation suggests that only ~15% of the fluctuations in ripple rate during the recognition process could be attributed to, or reflected by,

broader changes in HFB power. This further emphasizes the functional distinction between these two signals.

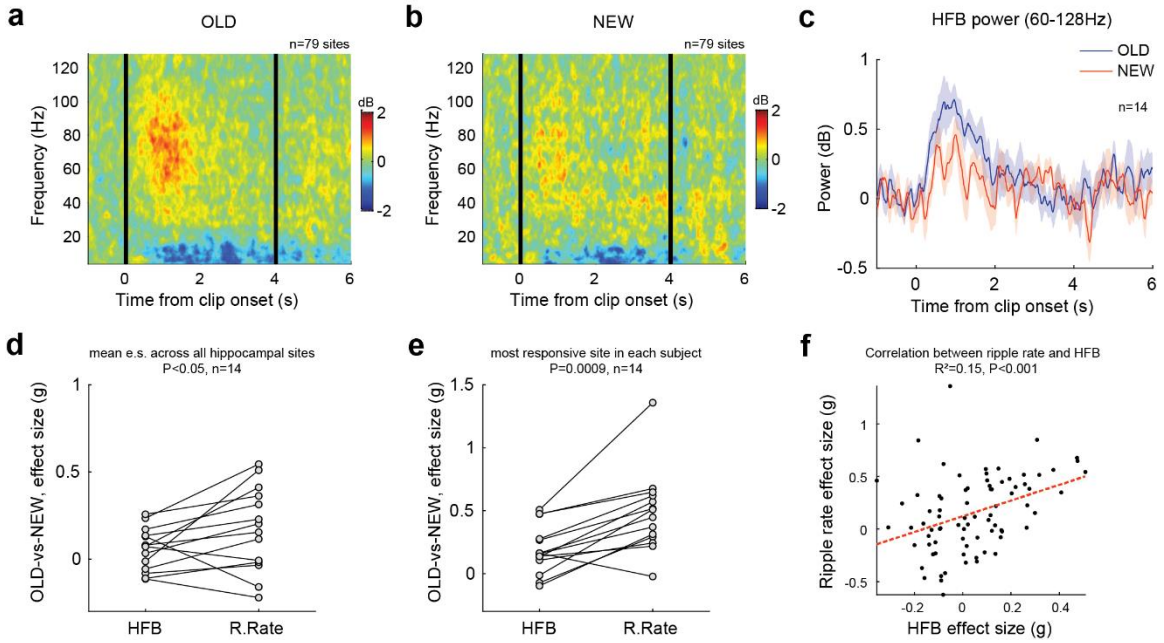

Figure 4 | Comparison between ripple rate and the HFB (high-frequency broadband) signal. The ripple rate shows greater sensitivity to the mnemonic process.

(a-b) Grand average spectrogram compute across all hippocampal sites, showing high-frequency broadband activity during clips recognized as OLD (a) and clips identified as NEW (b).

(c) Comparison between HFB power (60-128 Hz) during OLD and NEW clips. The difference between the two conditions failed to reach statistical significance (P=NS, n=14 patients, cluster-based permutation test).

(d) Comparison between the effect sizes of high-frequency broadband (HFB) and ripple rate for the "OLD-versus-NEW" contrast. The analysis, which averaged the effect sizes across all hippocampal sites in each patient, revealed a significantly larger effect size for ripple rate compared to HFB ($P<0.05$, n=14, Wilcoxon signed-rank test).

(e) Comparing the effect sizes obtained from the best HFB site and the best ripple-rate site in each patient. Again, a significantly larger effect size was observed for ripple rate compared to HFB (P=0.0009, n=14, Wilcoxon signed-rank test).

(f) The correlation between the effect sizes obtained from HFB and ripple rate signals.

Discussion

The present results confirm and extend our previous reports of the involvement of hippocampal ripples in memory processes along two major lines. First, they extend these findings to the domain of brain development during childhood and early adolescence (ages 6-14). Second, they extend the analysis to the

domain of naturalistic stimuli – watching a carton – which provides interesting insights into the distinct roles of ripples in various cognitive states encountered in everyday life.

Thus, our results reveal a striking selectivity in ripple activation while the young patients performed a passive on-line processing of a naturalistic movie as opposed to performing a recognition test on the same animated materials. This provides a clear indication that what activates the hippocampal ripples is not the mere momentary visual content of the movie – but rather the contextual situation in which this content is embedded. Two potential, not necessarily mutually exclusive, factors may account for this difference in ripple activation. The first possibility could be the switch from a continuous, ongoing processing during the movie presentation to a discrete event-like presentation of an isolated clip. Indeed, this possibility is compatible with previous research emphasizing the importance of abrupt cuts and event boundaries in hippocampal function (Ben-Yakov and Henson, 2018; Zheng et al., 2022). The second possible fact could be the cognitive task itself – which switched from passive processing of movie contents into an explicit recognition task in which participants were asked to actively recall the movie content and determine whether the presented movie clip was old or new to them.

Another, related, finding is the significant enhancement in ripple rate when patients were exposed to familiar movie clips compared to novel ones. This enhancement suggests that beyond the discreteness of the event and the overall decision-making task – there was a dimension of activation specifically related to the memory of the clips. Thus, this selectivity of ripple activation suggests that the hippocampal ripples are specifically involved with the active recall of previously stored materials as opposed to recognition attempts or mere processing of novel ones. This interpretation is nicely compatible with our earlier work demonstrating ripple activation when participant perform autobiographical memory judgments (Norman et al., 2021) as well as free recall of pictures (Norman et al., 2019). Importantly, these studies have shown that ripple activations were specific to the mnemonic processing and were not evident when other cognitively effortful tasks were employed (e.g., arithmetic calculations).

The substantial coverage and number of hippocampal recording sites allowed a coarse analysis of anatomical localization of the recognition effect. Our results did not show evidence for local clustering of preferential activation to old vs. new content within the hippocampus (Figure 3D). Rather, the results highlight the distributed nature of the hippocampal mnemonic representation, which is compatible with a similar observation made previously in an autobiographical and semantic memory recall (Norman et al., 2021). Yet, when comparing the hemispheric preferences – i.e., left versus right hippocampus – a significant left-hemisphere dominance was observed, aligning with our previous observations (Norman et al., 2021), as well as with a previous fMRI study showing a left-lateralized subsequent memory effect in children of a similar age tested on words (Maril et al., 2010). Although the memory test we employed was non-verbal in nature, it is still interesting to consider whether the observed left-hippocampus preference might be connected to the language dominance of the left hemisphere. However, further exploration of this notion

would necessitate a larger dataset and the inclusion of both verbal and non-verbal conditions (Golby et al., 2001).

High-frequency broadband (HFB) power has been established as a reliable index of local neuronal population activity in cortical systems (Manning et al., 2009; Miller et al., 2014; Nir et al., 2007; Parvizi and Kastner, 2018; Watson et al., 2018). However, far less is known about this collective neuronal activity marker in hippocampal neurophysiology. It should be noted that the HFB power modulation in the cortex is likely to stem from the functional clustering of neuronal response properties in the well-established cortical columns. The fact that no such clustering has been documented in the hippocampus – poses a challenge in interpreting the precise neuronal basis of HFB power in this region. Furthermore, it is not clear how much information overlap exists between hippocampal HFB and ripple rate – despite their derivation from similar, partially overlapping frequency bands in the local field potential (ripples: ~80-140 Hz, HFB: ~60-160Hz).

Indeed, our analysis revealed some overlap between the memory-related ripple rate changes and concurrent HFB power modulation (see Figure 4f). However, importantly, the ripple rate changes showed a significantly higher level of specificity – i.e., when comparing the preferential activation to old vs new content (Figure 4d-e). A likely explanation for these results is that the HFB and ripple rate may share a wide-spread, arousal-like, physiological modulations – leading to highly distributed increase in firing rates. However, specific contents such as the difference between old and new materials – may preferentially generate ripples while remaining unselective in terms of global neuronal activity in the hippocampus.

Conclusions. Our findings provide the first evidence for the involvement of hippocampal ripples in declarative memory processes in school-age children. The results indicate that the electrophysiological characteristics of hippocampal ripples (Norman et al., 2019, 2021) appears early in the developing brain. This was demonstrated in the ripple dynamics, ripple frequency, functional selectivity, and mnemonic specializations. Specifically, our findings highlight the early development of cognitive specificity in ripple activation, which shows notable selectivity towards explicit memory judgments in young children. This reinforces the notion that awake hippocampal ripples are closely tied to mnemonic processes that are consciously accessible and reportable (Henin et al., 2021; Kunz et al., 2022; Norman et al., 2019, 2021; Vaz et al., 2019), as opposed to the more automatic, sensory-driven components, that contribute to the sense of familiarity in a more implicit manner (Eichenbaum et al., 2007).

Acknowledgments. We express our gratitude to the patients and their families for their generous willingness to participate in this study. This work was supported in part by the Zuckerman STEM Leadership Program (YN) and by the CIFAR Tanenbaum Fellowship (RM).

Author contributions. YN, RM and ML conceived the study. YN designed the experiment. YN analyzed the data. RM and ML supervised the analysis. ML, SFS and GD performed the surgeries. YN and ML

installed the experimental setup. ML ran the experiment and supervised all aspects of data collection. MF and CB performed neurological and neuropsychological evaluations. DT, ND and MC monitored and analyzed epileptiform activity. YN, MH, and ML contributed to data curation and electrode localization. RM secured funding. YN and RM wrote the paper. ML further contributed to the writing by reviewing and editing the manuscript.

Competing interests. The authors declare no competing financial interests.

STAR ★ METHODS

KEY RESOURCES TABLE

REAGENT or RESOURCE	SOURCE	IDENTIFIER
Software and algorithms		
EEGLAB v2021.1	Delorme and Makeig, 2004	https://sccn.ucsd.edu/eeglab/index.php
FreeSurfer v7.2.0	Fischl et al, 2012	https://surfer.nmr.mgh.harvard.edu/fswiki
MES toolbox	Hentschke and Stüttgen, 2011	https://github.com/hhentschke/measures-of-effect-size-toolbox
iELVis toolbox	Groppe et al., 2017	http://ielvis.pbworks.com/w/page/116347253/FrontPage
Mass Univariate ERP Toolbox	Groppe et al., 2011	https://openwetware.org/wiki/Mass_Univariate_ERP_Toolbox
Custom-developed analysis code	N/A	10.5281/zenodo.8187953

Resource availability

Lead contact.

Further information and requests for resources should be directed to itzik.norman@gmail.com.

Materials availability.

This study did not generate any new reagents.

Data and code availability.

The data and code that support the conclusions are available upon reasonable request from YN (itzik.norman@gmail.com) and will be made publicly available on zenodo upon publication (DOI: 10.5281/zenodo.8187953).

Experimental Model and Subject Details

Participants. 14 children (8 females; age: M=9.4, range: 6-14; see Table S1 for additional demographic details) with medicine-resistant epilepsy were implanted (G.D, S.F and M.L) with intracranial stereo-electroencephalography (SEEG) electrodes (DIXI® and ALCIS®) as part of their pre-surgical evaluation at Rothschild Hospital, Paris. Electrode implantation was performed using ROSA (Zimmer©) under general anesthesia, regular anti-epileptic drugs, and antibiotics regimen. The location of the implanted electrodes was done based on the pre-surgical hypothesis and confirmed post-operatively by computed tomography (CT). The patients included in this study were selected based on electrode coverage in the hippocampus. Each patient was monitored in the hospital for 5 days on average (4-15 days). All patients had left hemispheric dominance for language, as determined pre-surgically using functional MRI and/or SEEG language mapping. The study was approved by the Institutional Review Board (TNP-SEEG protocol V1-0

20151012 1/6), and a written informed consent to participate in the study was obtained from the child's parents before surgery.

METHOD DETAILS

Intracranial EEG recordings. All electrophysiological data were recorded using a Micromed (Treviso, Italy) clinical monitoring system. Sampling rate was commonly 512 Hz (256 Hz in five patients) with a bandpass filter of 0.7-300Hz. None of the patients included in the analysis experienced any seizures throughout the experimental duration.

Experimental Task. The task began with a 3-min period of closed-eyes rest, after which the participants watched a 6.5-minute audiovisual pink panther cartoon titled "Pink Breakfast". After an additional 3-min resting state, participants re-watched the same cartoon. Upon completion of the second screening, the participants underwent an old/new recognition test. In this test, 40 short video clips, each lasting 4 seconds, were presented with no sounds. The clips were extracted either from the original cartoon (n=20; "Pink Breakfast") or from a different episode with similar food themes (n=20; "Dietetic Pink"). The participants were instructed to indicate whether each clip was old or new by pressing the left/right mouse buttons as soon as they had an answer. Participants that were unlikely to execute the button press in a timely manner were instructed to respond verbally instead, and the experimenter pressed the button on their behalf (a total of 6 patients). Throughout the task, the parents of the participants remained quietly at their bedside.

Electrode localization. Structural MRI were acquired using a (GE Healthcare 3 tesla SIGNA scanner) at the Rothschild Hospital. A preoperative T1-weighted 1mm isometric scan was co-registered to the post-operative CT through the procedure described previously (Norman et al., 2021), which is also extensively documented in the iELVis toolbox (Groppe et al., 2017). Individual recoding sites were identified visually on the co-registered CT, and were marked in each subject's preoperative MRI native space, using BioImage Suite (Papademetris et al., 2006). After processing the MRI in Freesurfer (Fischl, 2012) to segment the cortex and hippocampus (Iglesias et al., 2015), we superimposed the hippocampal electrodes onto a 3D reconstruction of the hippocampal formation, allowing us to determine the precise subfield localization of each recording site within the native space of the patient's brain.

Preprocessing and data analysis. Data analysis was performed in MATLAB 2021a (MathWorks Inc., Natick, MA) using EEGLAB v2021.1 (Delorme and Makeig, 2004) and custom-developed analysis code. The raw iEEG signal was examined statistically to identify and exclude noisy or corrupted channels from further analysis. Channels with voltage values, voltage derivatives, or RMS in the 99th percentile that were 5 standard deviations greater than the rest of the electrodes were marked for exclusion after visual inspection in the time and frequency domains. Preprocessing included converting all healthy iEEG channels into bipolar derivations. Electrodes in the hippocampus were referenced relative to a nearby white-matter

contact, that was identified anatomically using FreeSurfer's segmentation (Fischl, 2012). The obtained bipolar signals were then notch-filtered to remove 50 Hz power line interference using a zero-lag linear-phase Hamming-windowed FIR band-stop filter (3 Hz wide).

Hippocampal Ripples Detection. To detect hippocampal ripples, a slightly modified version of the method described in (Norman et al., 2021) was employed. This detection was conducted on electrodes located within <2 mm from the hippocampal subfields CA1, CA2, CA3 or subiculum, i.e., the main stations on the hippocampal output pathways where physiological ripple oscillations are most prominently observed (Chrobak et al., 1996; Oliva et al., 2016). We delineated and reconstructed the individual hippocampal subfields based on the structural MRI scans of the patients (Iglesias et al., 2015). Prior to ripple detection, a reference signal from a nearby white-matter contact was subtracted to eliminate common noise. The iEEG time series was then filtered between 70-180Hz (using a zero-lag linear-phase Hamming windowed FIR filter), and the instantaneous analytic amplitude was computed using a Hilbert transform. For the 5 patients with a sampling rate of 256 Hz, a narrower ripple-band filter between 70-128Hz was utilized. Based on our previously published procedure (Norman et al., 2021), extreme values were robustly estimated using Least-Median-Squares (LMS) (Seheult et al., 1989) and clipped to 4 SD above the mean to minimize ripple-rate induced biasing. The clipped signal was then squared and smoothed (Kaiser-window FIR low-pass filter with 40 Hz cutoff), and the mean and SD were computed across the entire experimental duration to define the threshold for event detection. Events from the original (squared but unclipped) signal that exceeded 4 SD above baseline were selected as candidate ripple events. Event duration was expanded until ripple power fell below 2 SD. Events shorter than 20ms or longer than 200ms were excluded. Adjacent events with less than 30ms separation (peak-to-peak) were merged. Finally, ripple peaks were aligned to the trough (of the non-rectified signal) closest to the peak power.

A control detection was performed on the common average signal computed across all iEEG channels. Hippocampal ripple events that coincided with common average ripple-band peaks were removed, thus avoiding erroneous detection of transient electrical and muscular artifacts that tend to appear simultaneously on multiple channels (Fiederer et al., 2016; Liu et al., 2022).

To distinguish between physiological ripples and other high-frequency oscillations (HFOs) related to epilepsy (Bragin et al., 2010), we discarded any candidate ripple event that occurred within 500 ms from inter-ictal epileptic discharges (IEDs). The detection of IEDs involved two complementary methods: an automated line-length algorithm based on (Baud et al., 2018) and a band-limited power analysis similar to (Smith et al., 2022). For the latter, the raw hippocampal iEEG signal was first filtered between 20-40Hz using a zero-lag linear-phase Hamming windowed FIR filter. Next, the filtered signal underwent rectification, squaring, smoothing, and z-scoring. Events that exceeded 8 standard deviations (SD) were identified as IEDs.

Statistical tests. All statistical analyses were performed in MATLAB. Pairwise comparisons were carried out using two-sided Wilcoxon signed-rank and rank-sum tests, unless stated otherwise. We did not use statistical methods to predetermine sample sizes, however, sample sizes were similar to those generally employed in the field (Helfrich et al., 2019; Norman et al., 2019, 2021; Vaz et al., 2019). Typically, the unit of analysis was individual patients. In cases where the units of analysis were individual electrodes, this was explicitly mentioned in the text. Resampling tests were carried out using either in-house MATLAB code or using established routines (Groppe et al., 2011) implemented in the Mass Univariate ERP Toolbox (OpenWetWare, 2015). Multiple comparisons correction was carried out using either the false discovery rate adjustment (FDR) (Benjamini and Yekutieli, 2001), or through cluster-based permutation tests (Groppe et al., 2011; Maris and Oostenveld, 2007).

Mixed effects analysis. Mixed-effects analyses were carried out in MATLAB using the fitlme.m function. The data were fitted with a random intercept model that included the relevant fixed factors, as well as a random factor of 'Electrode' nested within 'Patient'. The latter accounts for the fact that different participants contributed different numbers of electrodes to the analysis.

References

Baud, M.O., Kleen, J.K., Anumanchipalli, G.K., Hamilton, L.S., Tan, Y.L., Knowlton, R., and Chang, E.F. (2018). Unsupervised learning of spatiotemporal interictal discharges in focal epilepsy. Clin. Neurosurg. *83*, 683–691.

Ben-Yakov, A., and Henson, R.N. (2018). The hippocampal film editor: Sensitivity and specificity to event boundaries in continuous experience. J. Neurosci. *38*, 10057–10068.

Benjamini, Y., and Yekutieli, D. (2001). The control of the false discovery rate in multiple testing under dependency. Ann. Stat. *29*, 1165–1188.

Brown, T.T., and Jernigan, T.L. (2012). Brain development during the preschool years. Neuropsychol. Rev. *22*, 313–333.

Buzsáki, G. (2015). Hippocampal sharp wave-ripple: A cognitive biomarker for episodic memory and planning. Hippocampus *25*, 1073–1188.

Canada, K.L., Botdorf, M., and Riggins, T. (2020). Longitudinal development of hippocampal subregions from early- to mid-childhood. Hippocampus *30*, 1098–1111.

Chen, Y.Y., Aponik-Gremillion, L., Bartoli, E., Yoshor, D., Sheth, S.A., and Foster, B.L. (2021). Stability of ripple events during task engagement in human hippocampus. Cell Rep. *35*.

Chrobak, J.J., Buzstiki, G., Buzsáki, G., and Buzstiki, G. (1996). High-frequency oscillations in the output networks of the hippocampal-entorhinal axis of the freely behaving rat. J. Neurosci. *16*, 3056–3066.

Daugherty, A.M., Bender, A.R., Raz, N., and Ofen, N. (2016). Age differences in hippocampal subfield volumes from childhood to late adulthood. Hippocampus *26*, 220–228.

Daugherty, A.M., Flinn, R., and Ofen, N. (2017). Hippocampal CA3-dentate gyrus volume uniquely linked to improvement in associative memory from childhood to adulthood. Neuroimage *153*, 75–85.

Delorme, A., and Makeig, S. (2004). EEGLAB: An open source toolbox for analysis of single-trial EEG dynamics including independent component analysis. J. Neurosci. Methods *134*, 9–21.

Dickey, C.W., Verzhbinsky, I.A., Jiang, X., Rosen, B.Q., Kajfez, S., Stedelin, B., Shih, J.J., Ben-Haim, S., Raslan, A.M., Eskandar, E.N., et al. (2022). Widespread ripples synchronize human cortical activity during sleep, waking, and memory recall. Proc. Natl. Acad. Sci. U. S. A. *119*, 1–12.

Dosenbach, N.U.F., Nardos, B., Cohen, A.L., Fair, D. a, Power, D., Church, J. a, Nelson, S.M., Wig, G.S., Vogel, A.C., Lessov-schlaggar, C.N., et al. (2011). Prediction of Individua Brain Maturity Using fMRI. Science (80-.). *329*, 1358–1361.

Eichenbaum, H., Yonelinas, A.P., and Ranganath, C. (2007). The medial temporal lobe and recognition memory. Annu. Rev. Neurosci. *30*, 123–152.

Fernández-Ruiz, A., Oliva, A., de Oliveira, E.F., Rocha-Almeida, F., Tingley, D., Buzsáki, G., Oliveira, E.F. De, Rocha-Almeida, F., Tingley, D., Buzsáki, G., et al. (2019). Long-duration hippocampal sharp wave ripples improve memory. Science (80-.). *364*, 1082–1086.

Fiederer, L.D.J., Lahr, J., Vorwerk, J., Lucka, F., Aertsen, A., Wolters, C.H., Schulze-Bonhage, A., Ball, T., Aertsen, A., Schulze-Bonhage, A., et al. (2016). Electrical Stimulation of the Human Cerebral Cortex by Extracranial Muscle Activity:Effect Quantification with Intracranial EEG and FEM Simulations. IEEE Trans. Biomed. Eng. *63*, 1–1.

Fischl, B. (2012). FreeSurfer. Neuroimage *62*, 774–781.

Geng, F., Redcay, E., and Riggins, T. (2019). The influence of age and performance on hippocampal function and the encoding of contextual information in early childhood. Neuroimage *195*, 433–443.

Gennatas, E.D., Avants, B.B., Wolf, D.H., Satterthwaite, T.D., Ruparel, K., Ciric, R., Hakonarson, H., Gur, R.E., and Gur, R.C. (2017). Age-related effects and sex differences in gray matter density, volume, mass, and cortical thickness from childhood to young adulthood. J. Neurosci. *37*, 5065–5073.

Ghetti, S., and Angelini, L. (2008). The development of recollection and familiarity in childhood and adolescence: Evidence from the dual-process signal detection model. Child Dev. *79*, 339–358.

Ghetti, S., and Bunge, S.A. (2012). Neural changes underlying the development of episodic memory during middle childhood. Dev. Cogn. Neurosci. *2*, 381–395.

Ghetti, S., Demaster, D.M., Yonelinas, A.P., and Bunge, S.A. (2010). Developmental Differences in Medial Temporal Lobe Function during Memory Encoding. *30*, 9548–9556.

Gogtay, N., Nugent, T.F., Herman, D.H., Ordonez, A., Greenstein, D., Hayashi, K.M., Clasen, L., Toga, A.W., Giedd, J.N., Rapoport, J.L., et al. (2006). Dynamic mapping of normal human hippocampal development. Hippocampus *16*, 664–672.

Golby, A.J., Poldrack, R.A., Brewer, J.B., Spencer, D., Desmond, J.E., Aron, A.P., and Gabrieli, J.D.E. (2001). Material-specific lateralization in the medial temporal lobe and prefrontal cortex during memory encoding. Brain *124*, 1841–1854.

Groppe, D.M., Urbach, T.P., and Kutas, M. (2011). Mass univariate analysis of event-related brain potentials/fields I: A critical tutorial review. Psychophysiology *48*, 1711–1725.

Groppe, D.M., Bickel, S., Dykstra, A.R., Wang, X., Mégevand, P., Mercier, M.R., Lado, F.A., Mehta, A.D., and Honey, C.J. (2017). iELVis: An open source MATLAB toolbox for localizing and visualizing human intracranial electrode data. J. Neurosci. Methods *281*, 40–48.

Helfrich, R.F., Lendner, J.D., Mander, B.A., Guillen, H., Paff, M., Mnatsakanyan, L., Vadera, S., Walker, M.P., Lin, J.J., and Knight, R.T. (2019). Bidirectional prefrontal-hippocampal dynamics organize information transfer during sleep in humans. Nat. Commun. *10*, 1–16.

Henin, S., Shankar, A., Borges, H., Flinker, A., Doyle, W., Friedman, D., Devinsky, O., Buzsáki, G., and Liu, A. (2021). Spatiotemporal dynamics between interictal epileptiform discharges and ripples during associative memory processing. Brain 1590–1602.

Iglesias, J.E., Augustinack, J.C., Nguyen, K., Player, C.M., Player, A., Wright, M., Roy, N., Frosch, M.P., McKee, A.C., Wald, L.L., et al. (2015). A computational atlas of the hippocampal formation using ex vivo, ultra-high resolution MRI: Application to adaptive segmentation of in vivo MRI. Neuroimage *115*, 117–137.

Jadhav, S.P., Kemere, C., German, P.W., and Frank, L.M. (2012). Awake Hippocampal Sharp-Wave Ripples Support Spatial Memory. Science (80-.). *336*, 1454–1458.

Johnson, E.L., Tang, L., Yin, Q., Asano, E., and Ofen, N. (2018). Direct brain recordings reveal prefrontal cortex dynamics of memory development. Sci. Adv. *4*, eaat3702.

Joo, H.R., and Frank, L.M. (2018). The hippocampal sharp wave–ripple in memory retrieval for immediate use and consolidation. Nat. Rev. Neurosci. *19*, 744–757.

Khuvis, S., Yeagle, E.M., Norman, Y., Grossman, S., Malach, R., and Mehta, A.D. (2021). Face-selective units in human ventral temporal cortex reactivate during free recall. J. Neurosci. *41*, JN-RM-2918-19.

Kunz, L., Staresina, B.P., Reinacher, P.C., Brandt, A., Guth, T.A., Schulze-bonhage, A., and Jacobs, J. (2022). Ripple-locked coactivity of stimulus-specific neurons supports human associative memory.

Lavenex, P., and Banta Lavenex, P. (2013). Building hippocampal circuits to learn and remember: Insights into the development of human memory. Behav. Brain Res. *254*, 8–21.

Lenroot, R.K., Gogtay, N., Greenstein, D.K., Wells, E.M., Wallace, G.L., Clasen, L.S., Blumenthal, J.D., Lerch, J., Zijdenbos, A.P., Evans, A.C., et al. (2007). Sexual dimorphism of brain developmental trajectories during childhood and adolescence. Neuroimage *36*, 1065–1073.

Liu, A.A., Henin, S., Abbaspoor, S., Bragin, A., Buffalo, E.A., Farrell, J.S., Foster, D.J., Frank, L.M., Gedankien, T., Gotman, J., et al. (2022). A consensus statement on detection of hippocampal sharp wave ripples and differentiation from other fast oscillations. Nat. Commun. *13*.

Maingret, N., Girardeau, G., Todorova, R., Goutierre, M., and Zugaro, M.M. (2016). Hippocampo-cortical coupling mediates memory consolidation during sleep. Nat. Neurosci. *19*, 959–964.

Manning, J.R., Jacobs, J., Fried, I., and Kahana, M.J. (2009). Broadband Shifts in Local Field Potential Power Spectra Are Correlated with Single-Neuron Spiking in Humans. J. Neurosci. *29*, 13613–13620.

Maril, A., Davis, P.E., Koo, J.J., Reggev, N., Zuckerman, M., Ehrenfeld, L., Mulkern, R. V., Waber, D.P., and Rivkin, M.J. (2010). Developmental fMRI study of episodic verbal memory encoding in children. Neurology *75*, 2110–2116.

Maris, E., and Oostenveld, R. (2007). Nonparametric statistical testing of EEG- and MEG-data. J. Neurosci. Methods *164*, 177–190.

Miller, K.J., Honey, C.J., Hermes, D., Rao, R.P.N.P.N., denNijs, M., and Ojemann, J.G. (2014). Broadband changes in the cortical surface potential track activation of functionally diverse neuronal populations. Neuroimage *85*, 711–720.

Nir, Y., Fisch, L., Mukamel, R., Gelbard-Sagiv, H., Arieli, A., Fried, I., and Malach, R. (2007). Coupling between Neuronal Firing Rate, Gamma LFP, and BOLD fMRI Is Related to Interneuronal Correlations. Curr. Biol. *17*, 1275–1285.

Norman, Y., Yeagle, E.M., Khuvis, S., Harel, M., Mehta, A.D., and Malach, R. (2019). Hippocampal sharp-wave ripples linked to visual episodic recollection in humans. Science (80-.). *365*.

Norman, Y., Raccah, O., Liu, S., Parvizi, J., and Malach, R. (2021). Hippocampal ripples and their coordinated dialogue with the default mode network during recent and remote recollection. Neuron *109*, 1–14.

Ofen, N. (2012). The development of neural correlates for memory formation. Neurosci. Biobehav. Rev. *36*, 1708–1717.

Ofen, N., Kao, Y.C., Sokol-Hessner, P., Kim, H., Whitfield-Gabrieli, S., and Gabrieli, J.D.E. (2007). Development of the declarative memory system in the human brain. Nat. Neurosci. *10*, 1198–1205.

Oliva, A., Fernández-Ruiz, A., Buzsáki, G. retrievalyörgy G., and Berényi, A. (2016). Role of Hippocampal CA2 Region in Triggering Sharp-Wave Ripples. Neuron *91*, 1342–1355.

OpenWetWare (2015). Mass Univariate ERP Toolbox: Other EEG Analysis Software Packages --- OpenWetWare{,}.

Papademetris, X., Jackowski, M.P., Rajeevan, N., DiStasio, M., Okuda, H., Todd Constable, R., Staib, L.H., Constable, R.T., Staib, L.H., Todd Constable, R., et al. (2006). BioImage Suite: An integrated medical image analysis suite: An update. Insight J. *2006*, 209.

Parvizi, J., and Kastner, S. (2018). Promises and limitations of human intracranial electroencephalography. Nat. Neurosci. *21*, 474–483.

Power, J.D., Fair, D.A., Schlaggar, B.L., and Petersen, S.E. (2010). The Development of Human Functional Brain Networks. Neuron *67*, 735–748.

Riggins, T., Geng, F., Botdorf, M., Canada, K., Cox, L., and Hancock, G.R. (2018). Protracted hippocampal development is associated with age-related improvements in memory during early childhood. Neuroimage *174*, 127–137.

Rothschild, G., Eban, E., and Frank, L.M. (2017). A cortical-hippocampal-cortical loop of information processing during memory consolidation. Nat. Neurosci. *20*, 251–259.

Sakon, J.J., and Kahana, M.J. (2022). Hippocampal ripples signal contextually mediated episodic recall. Proc. Natl. Acad. Sci. *119*, e2201657119.

Schlichting, M.L., Guarino, K.F., Schapiro, A.C., Turk-Browne, N.B., and Preston, A.R. (2017). Hippocampal structure predicts statistical learning and associative inference abilities during development. J. Cogn. Neurosci. *29*, 37–51.

Seheult, A.H., Green, P.J., Rousseeuw, P.J., and Leroy, A.M. (1989). Robust Regression and Outlier Detection. (Wiley).

Seress, L., and zljak, L. (1992). Postnatal development of mossy cells in the human dentate gyrus: A light microscopic Golgi study. Hippocampus *2*, 127–141.

Shaw, P., Kabani, N.J., Lerch, J.P., Eckstrand, K., Lenroot, R., Gogtay, N., Greenstein, D., Clasen, L., Evans, A., Rapoport, J.L., et al. (2008). Neurodevelopmental trajectories of the human cerebral cortex. J. Neurosci. *28*, 3586–3594.

Shin, J.D., Tang, W., and Jadhav, S.P. (2019). Dynamics of Awake Hippocampal-Prefrontal Replay for Spatial Learning and Memory-Guided Decision Making. Neuron *104*, 1110-1125.e7.

Smith, E.H., Liou, J.Y., Merricks, E.M., Davis, T.S., Thomson, K., Greger, B., House, P.A., Emerson, R.G., Goodman, R.R., McKhann, G.M., et al. (2022). Title: Human interictal epileptiform discharges are bidirectional traveling waves echoing ictal discharges. Elife *11*, 1–20.

Staba, R.J., Wilson, C.L., Bragin, A., Jhung, D., Fried, I., and Engel, J. (2004). High-frequency oscillations recorded in human medial temporal lobe during sleep. Ann. Neurol. *56*, 108–115.

Tang, L., Pruitt, P.J., Yu, Q., Homayouni, R., Daugherty, A.M., Damoiseaux, J.S., and Ofen, N. (2020). Differential Functional Connectivity in Anterior and Posterior Hippocampus Supporting the Development of Memory Formation. Front. Hum. Neurosci. *14*, 204.

Le Van Quyen, M., Bragin, A., Staba, R., Crepon, B., Wilson, C.L., Engel, J., Quyen, M.L. Van, Bragin, A., Staba, R., Cre, B., et al. (2008). Cell Type-Specific Firing during Ripple Oscillations in the Hippocampal Formation of Humans. J. Neurosci. *28*, 6104–6110.

Vaz, A.P., Inati, S.K., Brunel, N., and Zaghloul, K.A. (2019). Coupled ripple oscillations between the medial temporal lobe and neocortex retrieve human memory. Science (80-.). *363*, 975–978.

van de Ven, G.M., Trouche, S., McNamara, C.G., Allen, K., and Dupret, D. (2016). Hippocampal Offline Reactivation Consolidates Recently Formed Cell Assembly Patterns during Sharp Wave-Ripples. Neuron *92*, 968–974.

Watson, B.O., Ding, M., and Buzsáki, G. (2018). Temporal coupling of field potentials and action potentials in the neocortex. Eur. J. Neurosci. *48*, 1–16.

Zheng, J., Schjetnan, A.G.P., Yebra, M., Gomes, B.A., Mosher, C.P., Kalia, S.K., Valiante, T.A., Mamelak, A.N., Kreiman, G., and Rutishauser, U. (2022). Neurons detect cognitive boundaries to structure episodic memories in humans. Nat. Neurosci. *25*, 358–368.

Table S1. Demographic information, hippocampal electrode count and seizure onset zone for each patient, related to STAR Methods

Subject	Gender	Age	Sampling Rate	Implanted Hemisphere	Seizure Onset Zone (Soz)	Handedness	Hippocampal sites
PP02	f	7.5	256 Hz	RH	Right temporo mesial	Right	7
PP03	m	11	512 Hz	RH	No seizures occurred	Right	5
PP04	f	6	512 Hz	RH	Right temporo mesial	Right	4
PP05	m	14	256 Hz	RH	Right premotor and SMA	Right	3
PP06	f	8	512 Hz	LH	Left temporo mesial	Right	5
PP07	f	14	512 Hz	RH	Right temporal pole	Left	14
PP08	m	11.5	512 Hz	LH	Left frontal and pre-frontal	Right	1
PP09	m	10	512 Hz	LH	Left fronto-temporo-insular	Left	7
PP10	m	6.5	512 Hz	LH	Left Temporo-parietal junction	Right	5
PP11	f	8.5	256 Hz	LH	Left multifocal	Right	6
PP15	m	9	256 Hz	LH	Left fronto-central	Right	5
PP16	f	6.5	256 Hz	RH	Unidentified	Right	3
PP17	f	11	256 Hz	RH	Right antero-temporo-mesial	Right	3
PP18	f	9	512 Hz	LH	Left fronto-polar-opercular	Right	11
TOTAL		**M=9.43**					**79**